FLUID INSTABILITIES TERM PROJECT: NUMERICAL ANALYSIS OF ONE INSTANCE OF THE KELVIN-HELMHOLTZ STABILITY PROBLEM

SETH JACOBSON, DEVIN SILVIA,
JESSE LORD, AND JOHN WONG

UNIVERSITY OF COLORADO, BOULDER, CO 80309

ABSTRACT. We present the results from a hydrodynamic simulation of the classic Kelvin-Helmholtz instability using TRIPLE. In this simulation, we examine the particular case of a flow with a Richardson number of 0.05 and a Reynold's number of 1500. We compare the outcome for both the two-dimensional and three-dimensional cases as well as the results of direct numeral simulation versus the large eddy approximation. We discuss various points in time during the simulation that appear to produce interesting behavior and what characteristics manifest themselves in this particular realization of the instability.

1. INTRODUCTION

The Kelvin-Helmholtz instability occurs at the shear interfaces between two flows with antiparallel velocities. In its simplest form the basic flow is two infinite, incompressible, horizontal streams of oppossing velocities and stratefied density placed one on top of the other. The instability grows as a sinusoidal disturbance which induces vorticity, and then acts to increase the motion, causing the fluid to go unstable. The flow forms large billows, which then collapse after turbulent structures form and disrupt the flow. The flow will reach a steady state with a turbulent boundary layer diffusing the shear between the flows.

During this series of events, there are numerous complex components. The first is that before the large scale billow collapses (and if the Richardson number is low enough), the center of the billow rotates as a solid body creating a reserve of potential energy that will be released once the billow can no longer support itself. The other is the creation of transverse structure across the breadth of the billow. Convective instability creates roll features aligned with the flow. These vortex tubes add extra structure to the flow and help support the billow.

Understanding Kelvin-Helmholtz instabilities are important because of the appearance of shear flows throughout nature. Numerous examples can be found in astrophysical applications such as disks and jets along with more nearby phenomena such as currents in the ocean, an example being surface waves, and atmosphere, an example being billow clouds. Our simulation is focused upon this application in particular. While the shear provides instability, the temperature and density gradients act to stabilize the flow. This can be thought of as inertia versus buoyancy. The stability of the atmosphere is quantified by the Richardson number.

$$Ri = \frac{g\alpha\beta h^2}{U_0^2} \tag{1}$$

Where g is the gravitational constant, alpha is $1/300$ K, βh is the temperature scale, h is the length scale, and U_0 is the velocity scale. Typical Richardson numbers that result in Kelvin-Helmholtz instabilities are $0 < Ri \leq 0.25$. Another important quantity of the flow is the Reynold's number.

$$Re = \frac{U_0 h}{\nu} \tag{2}$$

Where ν is the kinematic viscosity. The Reynold's number quantifies the importance of the inertial terms to the viscous diffusivity. A very analogous relation is the Peclet number:

$$Pe = \frac{U_0 h}{\kappa} \tag{3}$$

Where κ is a measure of the thermal diffusivity. The Peclet number quantifies the importance of the inertial terms to the thermal diffusivity. The Prandtl number is just a relation between the Peclet number and the Reynold number and is simply the viscosity over the thermal diffusivity.

In order to simplify the problem, the TRIPLE code uses the Boussinesq approximation, which means density fluctuations due to temperature only matter when attached to graviational terms. The non-dimensionalized equations of motion in the Boussinesq approximation become:

$$\partial_t \bar{u} + \bar{u} \cdot \Delta \bar{u} = \tag{4}$$

$$-\Delta(P + g\alpha\beta z^2/2) + Ri\theta\hat{z} + Re^{-1}\Delta^2\bar{u}$$

$$\partial_t \bar{\theta} + \bar{u} \cdot \Delta \bar{\theta} = -w + Pe^{-1} \Delta^2 \bar{u} \tag{5}$$

The flow is also assumed to be incompressible, so the divergence of the velocity is zero. The code represents all the field variables as series expansions with periodic boundary conditions for the transverse and longitudinal directions and the vertical has slippery boundaries. TRIPLE uses a spectral algorithm and a real fast fourier transform (no imaginary terms) to transfer between the physical and spectral spaces.

Our initial conditions were a velocity profile with a profile following a hyperbolic tangent function.

$$U = U_0 Tanh(z/h) \tag{6}$$

Where h is the length scale used for the problem and U_0 the velocity scale. The temperature profile was initially a linear gradient, and then the boundaries were held for the entire problem.

$$T = \beta z + \theta \tag{7}$$

Where βh becomes the temperature scale.

TRIPLE is a fully spectral code that takes full advantage of parallel processing power. For the direct numerical simulation (DNS), we used a grid of $600 \times 150 \times 600$. The LES code has a resolution of $200 \times 50 \times 200$. The 2-D runs has a resolution of 400×400. The code was run in these three settings to explore the pros and cons of each method. The 2-D code is able to capture some elements, however it cannot model vortex stretching and this has stark effects on the steady state it achieves.

The 3-D direct numerical simulation is able to capture vortex stretching, however its large grid size and ability to evolve small scale turbulence add accuracy as well as significant time. The large eddy simulation is designed to directly capture the large and mid scale turbulence with significant time savings but with a reduced grid is incapable of modeling the small scales. In order to correct for this effect, a spacial filter is applied to remove all small scales below some scale that is in the inertial range and then a turbulence model is used to add dissipation back into the system. This turbulence model must provide the right amount of energy flux at the cutoff in order to balance the energy contained in the simulation. Effectively, the LES code is attempting to replace the dissipation range of the kinetic energy spectrum with a faster to compute turbulence model than direct integration. This reduced gridsize, coupled with the spectral nature of the code also creates what are known as Gibbs oscillations, see figure 1. Since the spectra on this smaller gridsize are truncated, it creates gloabl errors. These errors are common in spectral codes with low resolution and are a significant source of uncertainty when using the LES as opposed to the DNS.

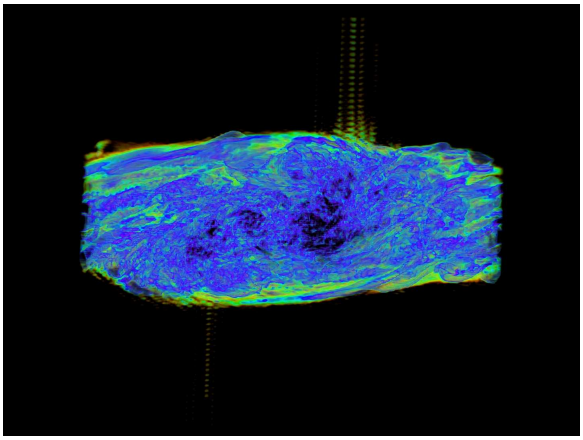

FIGURE 1. The LES at early time showing the Gibbs oscillations above and below the main structure

Throughout the rest of this paper, we will be discussing the effects seen during our simulation of a Kelvin-Helmholtz instability. We will also compare the results of the three different simulation techniques.

2. TIME EVOLUTION

Each of the three Kelvin-Helmholtz instability cases exhibited a laminar billow that gave way to turbulent instabilities. Our low Richardson number case had the most persistent billow, with overturning motion continuing out to a code time unit of at least 120 and some small remaining circulation in the center of the domain continuing to a code time unit of 180. In our case the turbulence begins outside the billow until it eventually consumes the domain, and we see long lasting laminar structures that do not occur in the high Richardson number case.

In figure 2 we can see the midplane average of the kinetic energy (solid) and the potential energy (dashed) versus code time units. This first figure shows the DNS while figure 3 shows the LES. We did not begin the LES until a code time unit of approximately 48. Since the LES simulates a dissipative region using sub-grid modelling, it cannot handle the laminar structure that exists during the early time evolution of our simulation. Thus, as we will see, the LES does a qualitativly similar job of simulating the instability once the domain has become turbulent, as is evident from these first two figures.

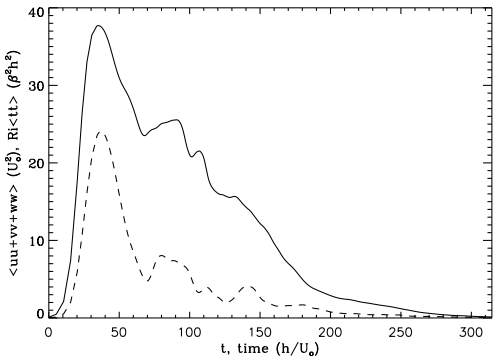

FIGURE 2. The DNS plot of kinetic energy vs time

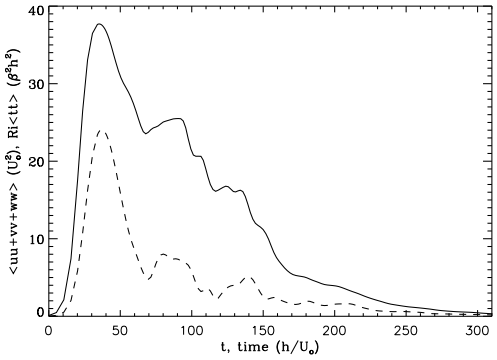

FIGURE 3. The LES plot kinetic energy vs time

In figure 2 we noticed three points of interest that we will explore in later sections. First is the maximum of the kinetic energy versus time plot, at a code time unit of approximately 35. At this point, the domain still strongly resembles a purely 2-dimenstional structure and begins to transition into a 3-dimenstional structure as it declines from the peak. Since we did not begin the LES until a later time, we cannot explore the differences between DNS and LES for this first kinetic energy peak.

The second point of interest is the second kinetic energy peak, which occurs at a code time unit of approximately 90. This second peak seems to correspond to the entire core of the billow going turbulent. We will see a similar peak in the time evolution of the kinetic energy in the 2 dimensional case, but this is the point at which the two dimensional simulation begins to significantly diverge from the 3 dimensional case.

The final interesting feature happens at a code time unit of 150.This is when the kinetic energy stops fluctuating and begins a consistent decline, but before it calms into its final state a code time unit of 190. At this time the DNS and LES still agree well but when examining the final state of the simulation it becomes clear that the LES does not allow as much dissipation as necessary. The heat flux in particular persists in the LES to a longer time than in the DNS. We also examine the 2 dimensional simulation, but it is clear from figure 4 that this case is simply oscillating and the lack of a third dimension prevents the vortex stretching and energy dissipation required for proper simulation of the instability. When examining the time series slices of y-vorticity in the 2 dimensional simulation it is clear that the billow persists and the turbulence never develops.

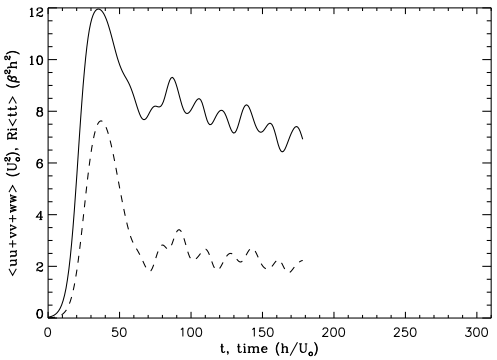

FIGURE 4. The 2D simulation plot of kinetic energy vs time

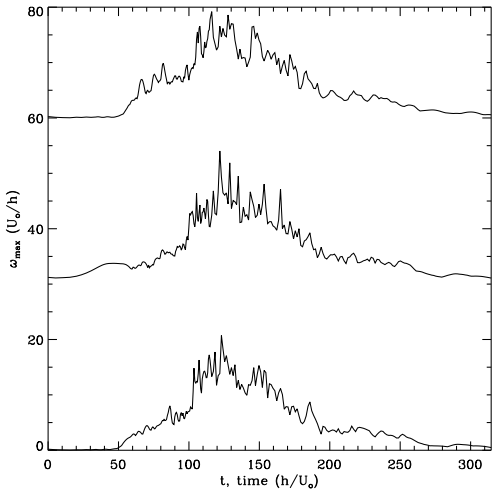

FIGURE 5. The DNS plot of maximum vorticity vs time

The final time evolution figures we introduce are the maximum vorticity in each dimension for the DNS and LES (note that the bottom is x, the middle is y, and the top is z, each offset by 30 vorticity units). In figure 5 we

see that there are large peaks in the maximum vorticity beginning near the second peak in the time evolution of the kinetic energy. When comparing this to figure 6, we can see that the smaller domain size of the LES prevents the small scale vortical structure present in the DNS and damps the maximum voriticty peaks.

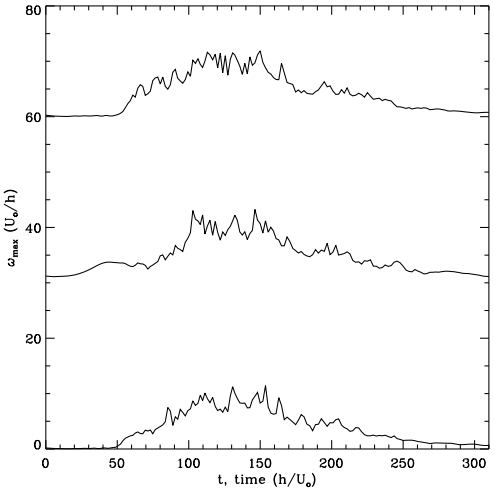

FIGURE 6. The LES plot of maximum vorticity vs time

From here, we move on to explore various "snapshots" of the simulations to try and get a handle on what sort of forces are at work in the K-H instability.

3. FIRST KINETIC ENERGY PEAK

In carrying out our analysis of the K-H instability produced by our particular set of initial conditions, we found it useful to investigate moments in time that seemed of particular significance or provided interesting insight in the behavior of the simulation.

To start off that investigation, we first explore the point in time when the kinetic energy of the system first peaks. For our specific case, we find that the first peak in the time evolution of kinetic energy occurs much earlier than the higher Richardson number cases, occuring at t $\sim$ 35 in units of code time as can be clearly seen in Figures 2, 3, and 4. It is important to note that both the 3D DNS run and 3D LES run were restarted off of the same set of initial conditions produced by a 3D DNS run and don't actually produce distinct results until after the first peak in kinetic energy has occured. For this reason, we will only be looking at the 2D and 3D DNS data.

One immediately notices that at this particular point in time the 2D and 3D runs are essentially indistinguishable. The flow has a firmly established solid-body rotation in the core with no significant turbulence. At this point the 3D volume is acting as a thick 2D plane as can be seen when one compares Figure 7 and Figure 8. We would also like to make a note to the reader that all of the snapshots of the 3D flows use a consistent color table throughout this paper.

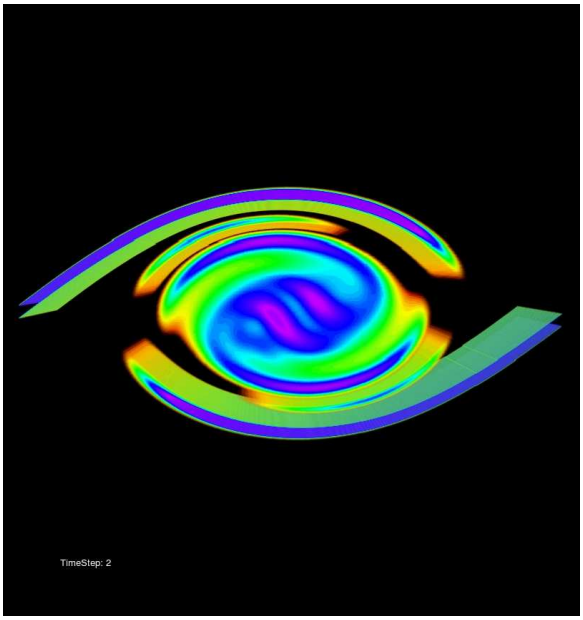

FIGURE 7. DNS first peak enstrophy snapshot

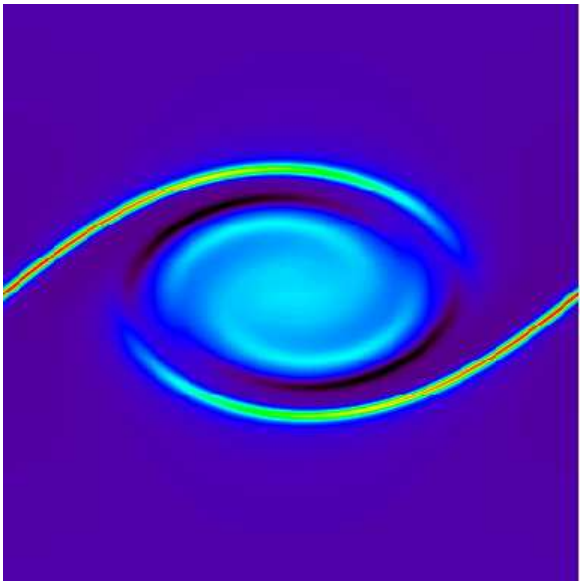

FIGURE 8. 2D first peak y-vorticity snapshot

Furthermore, one can compare the vorticity profiles as a function of height in the z direction between the the 2D and 3D cases (Figures 9 and 10) and again we

find that the simulations have produced nearly identical results. We will see shortly that it isn't until later times (our discussion of of the 2nd kinetic peak will show this) that the two flows diverge significantly.

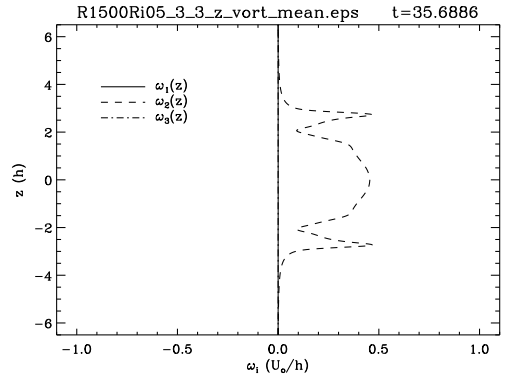

FIGURE 9. DNS first peak mean vorticity profile

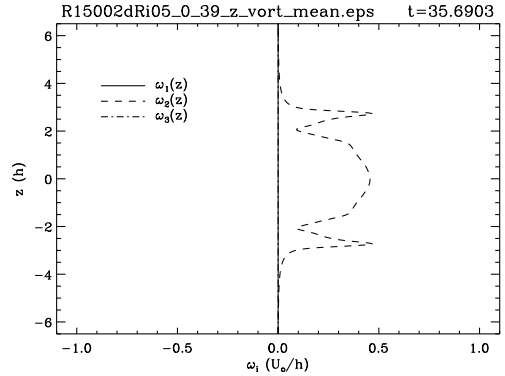

FIGURE 10. 2D first peak mean vorticity profile

Not surprisingly, when we analyzed essentially every imaginable quantity, we found resounding similarity in the 2D and 3D cases and as a result spare the reader the time that one might spend looking at nearly identical plots. We conclude, that in the situation where the 3D K-H instability is initialized as a 2D planar flow, it takes a significant length of time (nearly one-fifth of our total run time) for turbulence to develop in the 3D simulation and break down the symmetries present in the 2D case.

Outside of doing a direct comparison between the 2D and 3D cases, we can also explore the general nature of the instability by looking at vertical profiles of various quantities. For example, while the flow is undergoing this solid-body rotation there is rapid transport of material from the top of the flow down to the bottom and vice-versa as the fluid layers overturn. This is a high amount of heat flux, as can be seen in Figure 11, which starts pushing the temperature profile away from its linear initial condition to be more isothermal in the center as indicated by Figure 12.

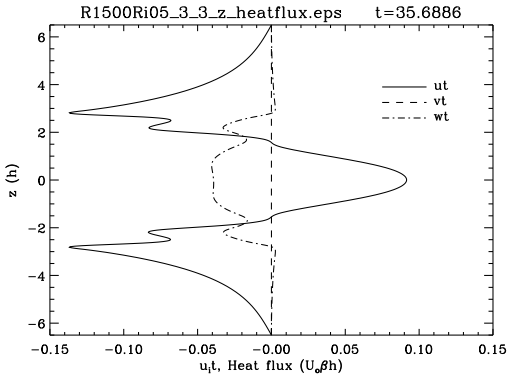

FIGURE 11. DNS first peak heatflux profile

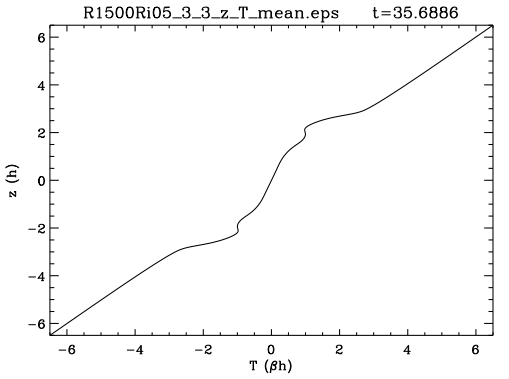

FIGURE 12. DNS first peak mean temperature profile

In ending our analysis of this first peak in the kinetic energy, we examine the energy spectrum seen in Figure 13. We see that the simulation exhibits a $k^{-\frac{5}{3}}$ inertial range as expected by Kolmogorov theory to a k_x of $\sim$20. After that, the spectrum drops off into the dissipation range where energy flows out of the system. One point to note is that at this early time before 3D vortex tube stretching has occurred, the relative amount of energy in the y-direction is much less than the other two directions as the flow has not yet evolved to being fully 3D in nature as mentioned above. We will see that this is no longer the case in later times.

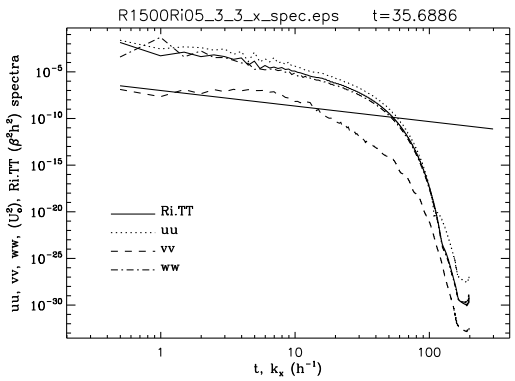

FIGURE 13. DNS first peak kinetic energy spectra in the x direction

4. SECOND KINETIC ENERGY PEAK

At the second peak of the kinetic energy spectrum, the core of the billow becomes turbulent in both 3D cases (fig 14) and continues to exhibit solid body rotation in the 2D simulation. Some vortex tubes are still visible along the edge of the flow in all three simulations extending from both sides of the domain towards the top and bottom edges of the billow.

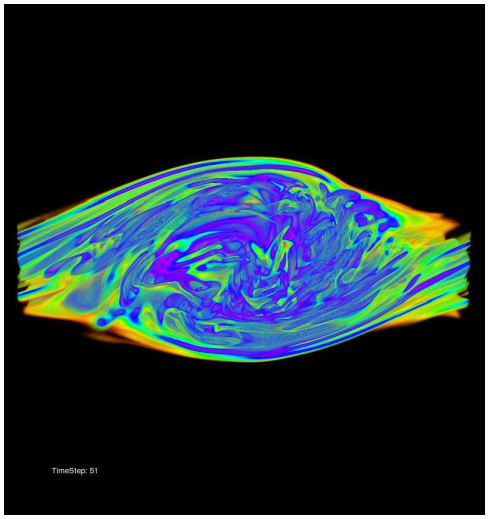

FIGURE 14. DNS second peak reynolds stress profile

The energy spectra for all three simulations show matching profiles as well. All three exhibit the $k^{-\frac{5}{3}}$ slope within the inertia range as predicted by the Kolmogorov spectrum. This is different from earlier times where the energy spectra in the y direction is strikingly different from x and z. Within the dissipation range at higher frequencies, both DNS and 2D show significant drops in the spectra whereas none is observed in the LES simulation. This is because the LES implementation truncates around the inertial range with no energy transfer to smaller scale for dissipation through viscosity.

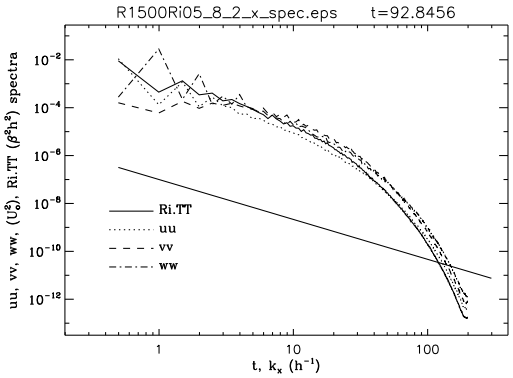

FIGURE 15. DNS second peak kinetic energy spectra in the x direction

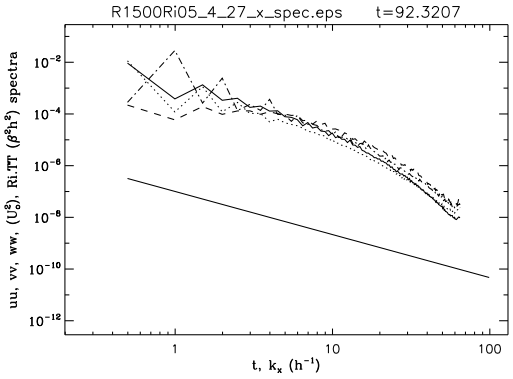

FIGURE 16. LES second peak kinetic energy spectra in the x direction

Vertical mean temperature profiles for all three are identical (fig 18). They all increase linearly with height with two separate kinks corresponding to the top and bottom half of the billows. In the middle is an inflection point with an isothermal profile. This feature is present in all three cases. Mean horizontal heat flux ut minima observed at the top and bottom edges of the billow from the first peak are still visible during this time step (fig 19). However, the positive maximum at $z = 0$ from earlier times has now been reduced to almost zero in all three simulations. Such flux profile sets up a larger heat gradient which will later be eliminated through mixing.

The vertical profiles for the mean production terms $-uw \cdot dU/dz$ are less correlated. The production term

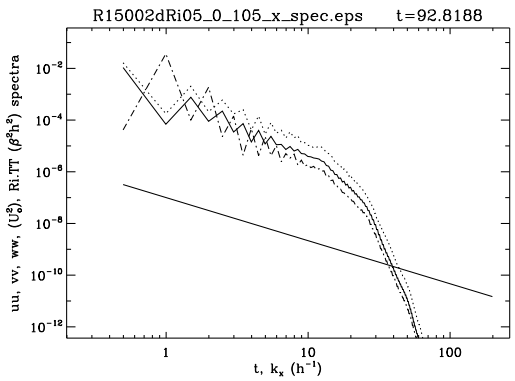

FIGURE 17. 2D second peak kinetic energy spectra in the x direction

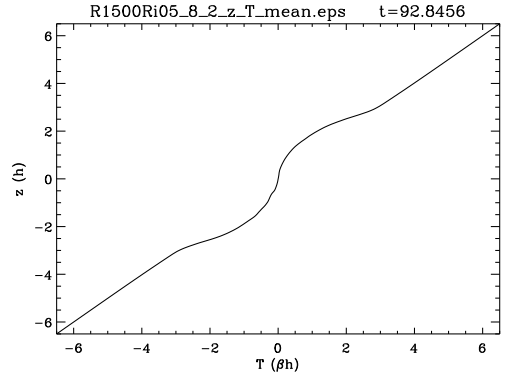

FIGURE 18. DNS second peak mean temperature profile

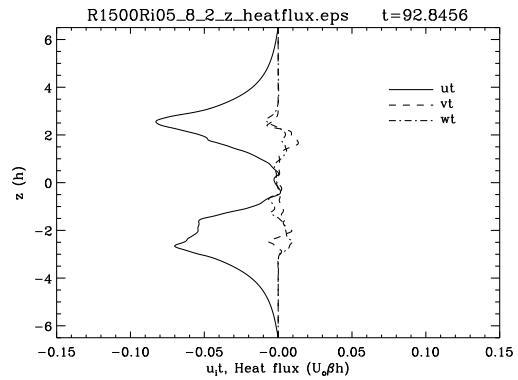

FIGURE 19. DNS second peak heatflux profile

for the 2D case (fig 20) is strictly negative with a rather prominent minimum at $z = 0$. For the LES run (fig 21), a positive maximum is observed instead, and the top and bottom edge of the billow are slightly negative. Finally, the DNS simulation (fig 22) shows a similar profile to the LES profile but with a smaller magnitude and more noisy. This discrepancy can be explained by the persisting billow core in the 2D case and turbulence in both 3D cases.

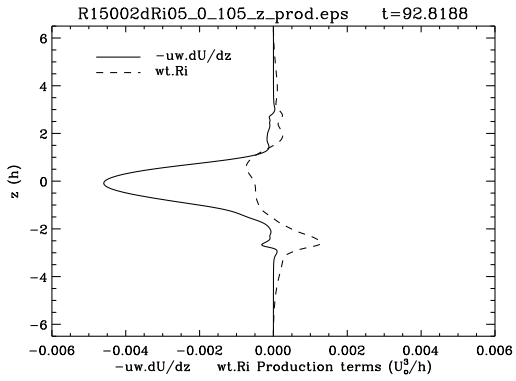

FIGURE 20. 2D second peak production terms profile

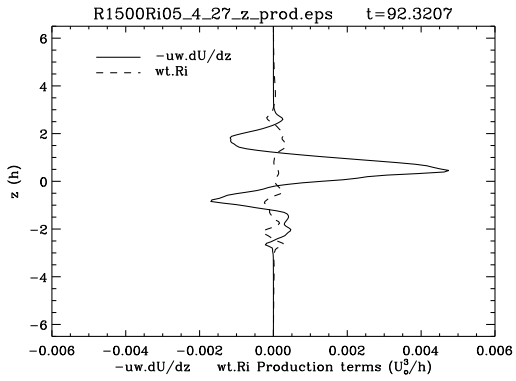

FIGURE 21. LES second peak production terms profile

5. KINETIC ENERGY DECLINE

Now we will examine the third feature mentioned when discussing figure 2 at a code time unit of 150. As we can see in figure 23 that the domain is fully turbulent with very little evidence of circulation except in the very center of the domain where there is some small right handed curl. In figure 24 we can see similar qualitative results with some tube like structure at the edge of the domain in both cases.

From figure 25 we can see the kinetic energy spectrum in the x direction. It appears that at this time the inertial range exists from approximately $k_x = 4$ to $k_x =$

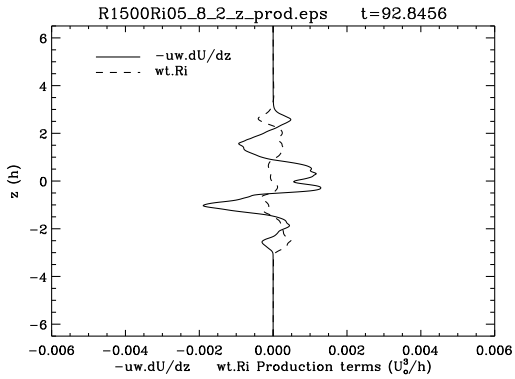

FIGURE 22. DNS second peak production terms profile

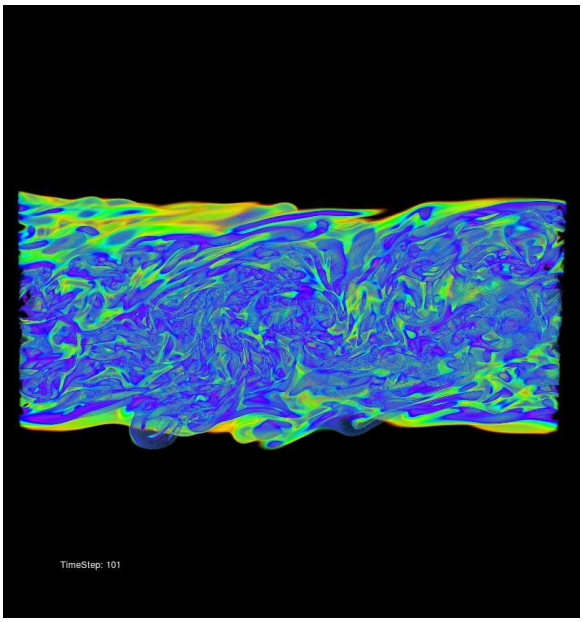

FIGURE 23. DNS kinetic energy decline enstrophy snapshot

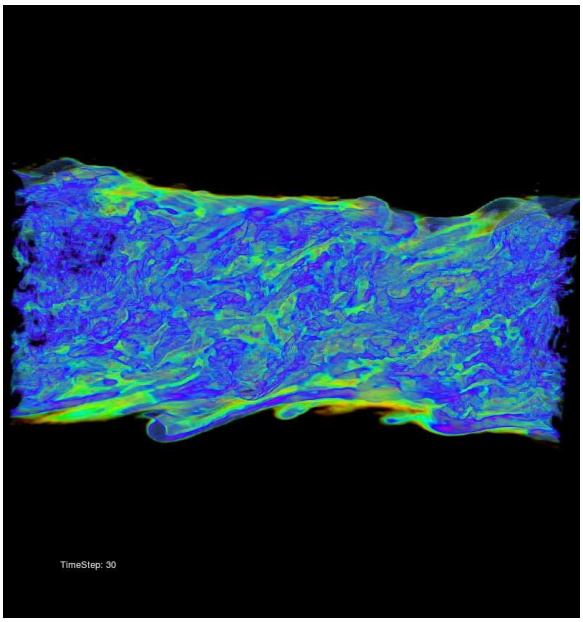

FIGURE 24. LES kinetic energy decline enstrophy snapshot

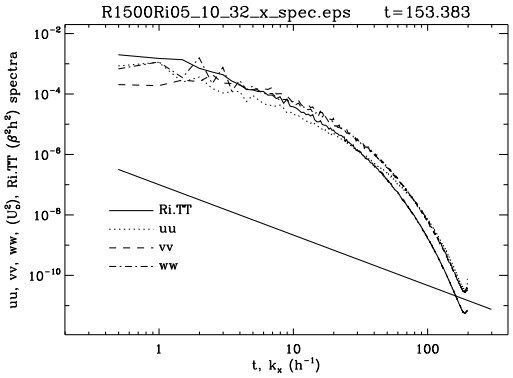

FIGURE 25. DNS kinetic energy decline KE spectra in the x direction

20. We see a similar result for the LES but it still has a small piece of the dissipation range, which could cause problems since the code is intended to run only in the inertial range. Since the 2 dimensional simulation cannot dissipate energy, the 2D spectrum at this time is not significantly different than in figure 17. Energy builds up in the middle of the spectrum and there is no obvious inertial range.

One of the most important characteristics of our simulation at late time is how long it takes to dissipate the heat flux. Figure 26 shows the heat flux for the DNS, which is qualititatively similar to the LES. The heat flux profile for this later time shows flux is now positive at $z = 2$ and $z = -2$, as opposed to earlier plots. This is likely because the mean temperature profile, figure 27, has reached its maximum distortion from the linear profile and the heat flux is now trying to restore the initial conditions. This mean temperature profile is very similar to the LES and persists into the later times examined in the next section.

The shear production (solid line), shown in figure 28, exhibits much larger values around $z = 0$ and is positive, indicating that the shear is working to dissipate energy from the turbulence at these late times, as expected. By this time the buoyancy term (dashed line) is nearly zero and no longer has a significant impact on the structure of the instability.

In figure 29, it is clear that the mean velocity profile for the x direction velocity still shows significant deviations from the original $tanh$ profile. Along with the

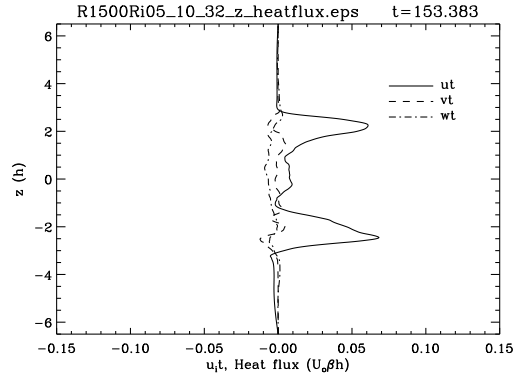

FIGURE 26. DNS kinetic energy decline heatflux profile

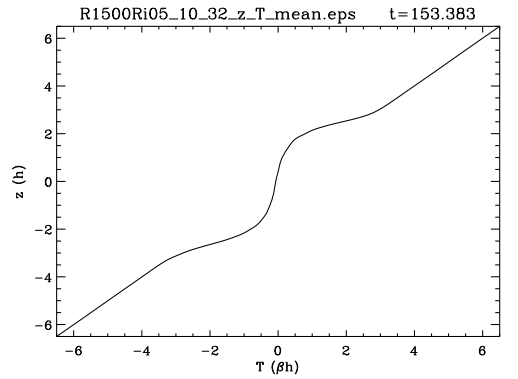

FIGURE 27. DNS kinetic energy decline mean temperature profile

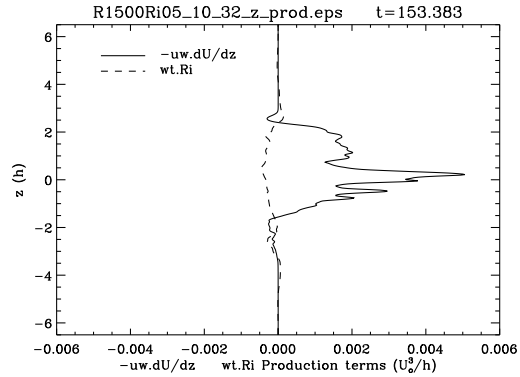

FIGURE 28. DNS kinetic energy decline production terms profile

mean temprature profile, these deviations demonstrate there is still a fossil of the instability even after the apparent overturning motion has stopped.

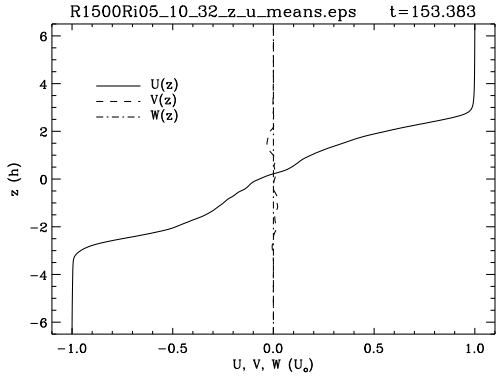

FIGURE 29. DNS kinetic energy decline mean velocity profile

Finally, we can see from the shear and buoyancy production terms in the 2 dimensional case, figure 30, that these two are nearly balanced. This indicates, as we have discussed previously that there is no energy dissipation and only a transfer from kinetic to potentional as the elliptical central region of the billow rotates.

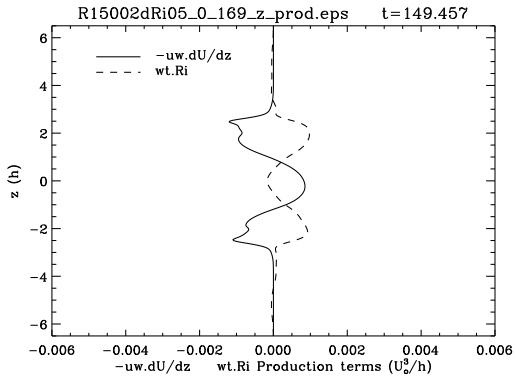

FIGURE 30. 2D late time shear and buoyancy production terms profile

6. LATE TIME BEHAVIOR

After the decay of the turbulence we still see some remnant structure in the mean temperature profile, figure 31, that does not occur in the high Richardson number case. These are the last timesteps for the DNS at code time unit 314.60. Notice that while our kinetic energy peaks at an earlier time than either of the other, higher Richardson number cases, we also see longer lasting perturbations to the mean temperature profile even after all the other profiles have decayed to zero.

The LES simulation was run to a much later time of 868.111 in code time units. We can see in figure 32 that

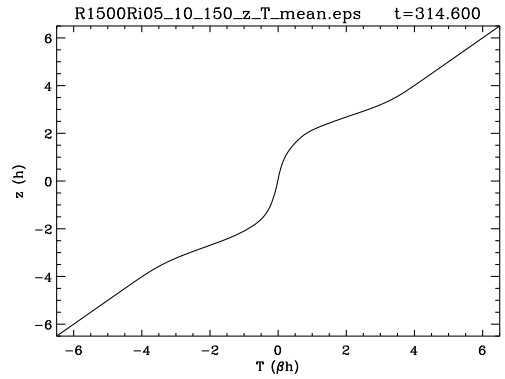

FIGURE 31. DNS final timestep mean temperature profile

these deviations from the original profiles decay but persist to very late in the simulation. This may be decieving because the LES does not dissipate energy as quickly as the DNS but it clearly takes a long time for the domain to re-establish the mean temperature profile.

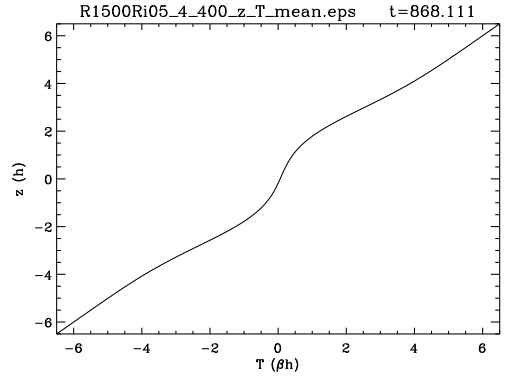

FIGURE 32. LES final timestep mean temperature profile

One of the main reasons that the temperature profile does not decay is that the heat flux becomes very small at late times. We can observe the beginning of this decreasing heat flux by comparing figures 26 and 33.

The heat flux continues to decrease until, at the final timestep, it is almost zero. Figure 34 shows the final timestep of the DNS run, which explains the non-linear temperature profile.

Figures 35 and 36 show similar heat flux profiles for the LES as the DNS profiles above. Notice that the LES profiles take significantly longer to decay to the same heat flux. This is the clearest indication that the dissipation is not as efficient for the LES as DNS and might

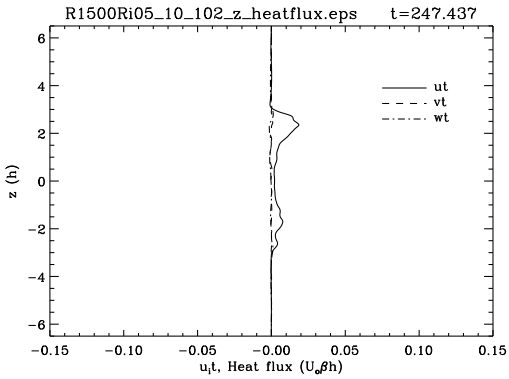

FIGURE 33. DNS late time heat flux profile

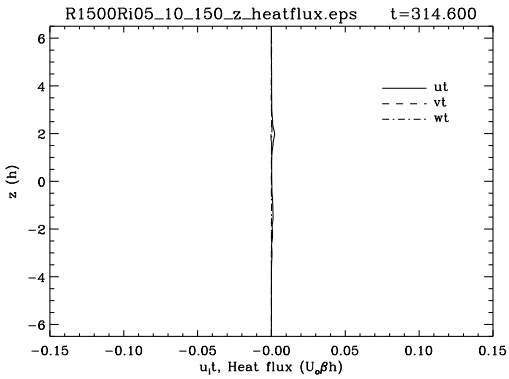

FIGURE 34. DNS final timestep heat flux profile

explain why the temperature profile has not become linear in 32.

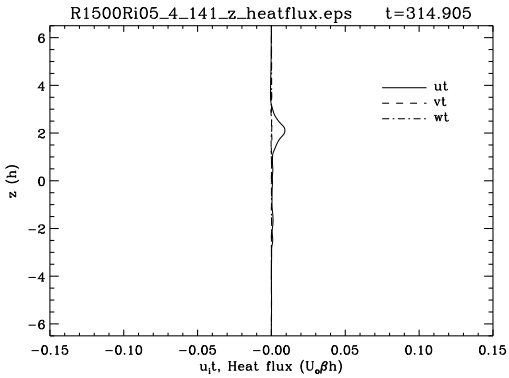

FIGURE 35. LES late time heat flux profile

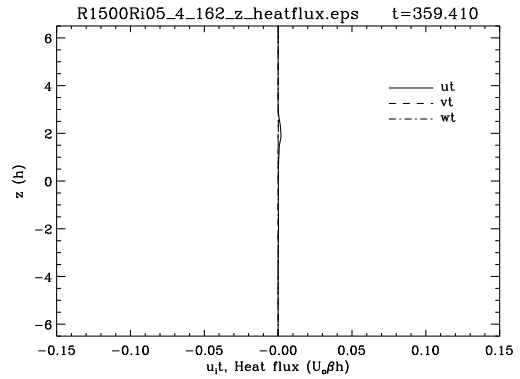

FIGURE 36. LES similar to final timestep of DNS heat flux profile

7. CONCLUSION

Kelvin-Helmholtz instabilities are seen in a variety of places in nature. Three dimensional simulations of these instabilities has given us greater insight into their properties.

Our examination of the Richardson number 0.05 case, can help explore the parameters and try to connect natural events to the simulations that we can explore more completely. For this low Richardson number we see long lasting laminar structures with the billow overturning multiple times before turbulence can begin to disrupt these structures. Even after the domain has become completely turbulent we see persistent circular motion where the billow used to be located. We also see remnants of this instability in the nearly isothermal center of the layer. Using these properties we can hopefully better understand what makes these characterstic cloud formations, and ocassionally causes our normally quiet sky to give us a bumpy reminder of its dynamical behavior.

ACKNOWLEDGEMENTS

Our group (infamously known as Team α) would like to thank Joe Werne for his assistance in running TRIPLE, producing analysis plots, and giving us a taste of computational modeling of fluid instabilities. We also thank John Clyne for providing us with a short tutorial on the usage of Vapor so that we could visualize our simulation in a three dimensional realm. Extending our thanks further, we recognize Juri Toomre as instructor of the course and the person who was able to get everything to come together to make this project happen. And finally, we thank Lord Kelvin and Hermann Ludwig Ferdinand von Helmholtz who graciously lended their names to this fascinating instability.